

# Road map through the desert: unification with vector-like fermions

Kamila Kowalska and Dinesh Kumar

*National Centre for Nuclear Research*

*Pasteura 7, 02-093 Warsaw, Poland*

## Abstract

In light of null results from New Physics searches at the LHC, we look at unification of the gauge couplings as a model-building principle. As a first step, we consider extensions of the Standard Model with vector-like fermions. We present a comprehensive list of spectra that feature fermions in two distinct  $SU(3)_C \times SU(2)_L \times U(1)_Y$  representations, in which precise gauge coupling unification is achieved. We derive upper and lower limits on vector-like masses from proton decay measurements, running of the strong gauge coupling, heavy stable charged particle searches, and electroweak precision tests. We demonstrate that due to a particular hierarchy among the mass parameters required by the unification condition, complementarity of various experimental strategies allows us to probe many of the successful scenarios up to at least 10 TeV.

---

\*kamila.kowalska@ncbj.gov.pl

†dinesh.kumar@ncbj.gov.pl

# 1 Introduction

Unification of three fundamental forces of the Standard Model (SM) into a single gauge interaction has been an enticing idea since the mid 1970s [1, 2, 3, 4, 5]. It emerged as a natural continuation of intellectual efforts that, in merging apparently unrelated phenomena, sought the key to a deeper understanding of nature, first by combining electricity and magnetism into a unified description, later leading to the establishment of the electroweak theory. Although the concept of unification as an underlying organizing principle stems to some extent from a sense of aesthetics, it finds a more robust justification in the fact that the renormalized gauge couplings of the SM, while evaluated at higher and higher energies, seem to converge towards a common value. This behavior might be understood as a manifestation of a new, unified description of fundamental interactions known as Grand Unified Theory (GUT).

Precise gauge coupling unification, however, is not really achieved in the SM as discrepancies among the GUT-scale values of the SM couplings reach several percent. To make it work, the particle spectrum needs to be extended in order to modify the renormalization group (RG) running of the couplings below the GUT scale.<sup>1</sup> Supersymmetry (SUSY) has the advantage of leading to gauge unification in a quite natural way, yet no experimental evidence of the low-scale SUSY has been found so far. While this fact does not undercut it completely as a theoretical framework, it is timely to ask to what extent unification of the gauge couplings is a unique property among various extensions of the SM. In other words, how many different beyond-the-SM (BSM) scenarios can be found whose particle spectrum differ quantitatively from the one of SUSY, and still allow for precise unification.

In addressing this question we would like to remain as generic as possible. On the other hand, a truly comprehensive study of all imaginable SM extensions would be a highly challenging (if not impossible) task. For that reason our approach will be incremental: we are going to begin with a relatively simple BSM setup, which will then be gradually extended to encompass more complex structures. It is in this spirit that we regard the issue of unification as a long term research project, a *road map* that would guide the model building through the desert between the electroweak (EW) and GUT scales.

We begin with defining the common framework for any unification analysis that we are going to undertake. The most important requirement is that the SM gauge symmetry persists up to the unification scale. It means, we will not consider Pati-Salam [2] or trinification [11, 12] type of GUTs as they do not require simultaneous unification of all three SM gauge couplings. For theoretical consistency, we also demand perturbativity of the renormalized model parameters up to the GUT energies.

Now we are going to make several additional assumptions, which on the one hand will substantially simplify the analysis, on the other will restrict the types of BSM scenarios that will be considered. Therefore, such assumptions may be dropped in the future studies. The additional requirements we impose are the following: (i) any extension of the SM must be anomaly free; (ii) scenarios with low scale unification,  $M_{\text{GUT}} \lesssim 10^{15}$  GeV, are not allowed (i.e. general dimension-6 operators leading to proton decay are not forbidden by

---

<sup>1</sup>In principle, the GUT-scale values of the couplings can also be modified by high-scale threshold corrections [6, 7, 8, 9]. These corrections, however, are strongly model dependent and for a certain range of the GUT-particle masses they become negligibly small [10]. Therefore, we neglect the effects of GUT threshold corrections throughout this study.

any additional mechanism [13]). Since the first condition restricts possible BSM particles to vector-like (VL) fermions and scalars, for the sole purpose of the current study (iii) we will only consider VL extensions of the SM.

The issue of gauge coupling unification in the presence of VL fermions is not a new idea and it received a lot of attention in the literature, both before the launch of the LHC [14, 15, 16, 17, 18, 19, 20, 21, 22, 23], and after [24, 25, 26, 27, 28, 10]. Similar analyses within the SUSY framework were performed as well [29, 30, 31, 32, 33, 34, 35, 36]. In most of the former studies only particular types and a limited number of VL representations were considered. In this regard Ref. [14] took a more generic approach and looked at 84 different  $SU(3)_C \times SU(2)_L \times U(1)_Y$  charge assignments for BSM fermions and scalars. Relatively recently the first attempt has been made in Ref. [28] to systematically study all possible VL extensions of the SM, in which BSM matter multiplets form incomplete representations of  $SU(5)$ . Scenarios with two distinct representations (and no more than six VL pairs in each of them) were considered, while independent VL masses were limited to 5 TeV.<sup>2</sup>

In the present work, we build on the findings of Ref. [28] and extend their analysis in several different directions. First of all, we boost the allowed mass range of VL fermions up to 10 TeV. While it may seem far beyond the reach of modern colliders, we will show that due to a particular hierarchy among the VL spectra allowing for unification, as well as to complementarity of various experimental strategies, one is actually able to derive exclusion lower bounds even on multi-TeV masses. Secondly, we do not *a priori* limit the maximum number of VL pairs in each representation. It turns out that, when this extra condition is discarded, novel solutions with respect to Ref. [28] can be found. Finally, we thoroughly discuss a variety of experimental methods that allow one to test the successful unification scenarios. We derive upper and lower limits on VL masses from proton decay measurements, running of the strong gauge coupling, heavy stable charged particle searches, and EW precision tests. We demonstrate that by combining independent experimental results we manage in many cases to probe (and to exclude) essentially the whole parameter space of a given model.

The paper is organized as follows. In Sec. 2 we define the fundamental building blocks of our BSM scenarios in terms of the transformation properties of VL fermions under the SM gauge symmetry group. Sec. 3 presents the main results of the study: a comprehensive list of representations that allow for unification of the SM gauge couplings. In Sec. 4 we discuss in detail experimental bounds that constrain the parameter space of the successful scenarios. We present our conclusion in Sec. 5. Technical details of the analysis are collected in two appendices.

## 2 Generic BSM scenarios with VL fermions

We begin our discussion with constructing a set of generic extensions of the SM that satisfy the requirements defined in the introduction, i.e. no extra gauge symmetry is imposed,

---

<sup>2</sup>Results for 3- and 4-representation scenarios and the VL mass fixed at 1 TeV were shown in Ref. [28] as well. However, as we will demonstrate in the present study, mass hierarchy among various VL representations is one of the main factors of the successful gauge coupling unification. For this reason, the fixed-mass analyses can not be considered comprehensive.

$R_2 \backslash R_3$	1	3	6	8
1	$\infty$	24	4	4
2	28	8	2	2
3	6	2	0	0
4	2	0	0	0

Table 1: Maximal number of VL fermions with the mass of 10 TeV, which allows for perturbative gauge couplings below  $10^{15}$  GeV.  $Y_F = 0$  is assumed.

$R_2 \backslash R_3$	1	3	6	8
1	$3\frac{1}{6}$	$1\frac{5}{6}$	$1\frac{1}{6}$	$1\frac{1}{6}$
2	$2\frac{1}{3}$	$1\frac{1}{3}$	$\frac{5}{6}$	$\frac{2}{3}$
3	$1\frac{5}{6}$	1	0	0
4	$1\frac{2}{3}$	0	0	0

Table 2: Maximal value of the hypercharge, which allows for perturbative gauge couplings below  $10^{15}$  GeV ( $N_F = 2$  and the VL mass is set at 10 TeV).

the only new particles in the spectrum are VL fermions, and the renormalized couplings remain perturbative at the unification scale. We additionally assume for the purpose of this study that any Yukawa interactions generated by the BSM sector and allowed by the gauge symmetry are negligible.<sup>3</sup>

We thus introduce  $N_{F_i}$  copies of new fermionic fields, which transform under the  $SU(3)_C \times SU(2)_L \times U(1)_Y$  gauge group as VL multiplets

$$(R_{3F_i}, R_{2F_i}, Y_{F_i}) \oplus (\bar{R}_{3F_i}, \bar{R}_{2F_i}, -Y_{F_i}). \quad (1)$$

Note that we count separately over both components of the pair, so  $N_{F_i}$  can only assume even values (with an exception of fermions that transform in an adjoint representation of a non-abelian gauge symmetry group). The index  $i$  runs over the number of distinct representations. At this stage both  $i$  and  $N_{F_i}$  are unconstrained.

Upper bounds on the dimension of possible VL representations and on the number of fermions that transform accordingly are provided by perturbativity condition. Let us first consider the SM extended by one representation of VL fermions and assume  $Y_F = 0$ . For various combinations of  $R_3$  and  $R_2$  and increasing number of VL copies, we run the SM gauge couplings from the low-energy scale, which we identify with the top quark mass  $M_t$  and at which the couplings assume the following values [37]

$$g_3(M_t) = 1.16660, \quad g_2(M_t) = 0.64779, \quad g_Y(M_t) = 0.35830, \quad (2)$$

up to  $10^{15}$  GeV.<sup>4</sup> The VL mass is fixed at 10 TeV as this is the largest allowed value of this parameter considered in the present study. RG equations (RGEs) for the gauge couplings in a general quantum field theory are well known [38] and we summarize their explicit two-loop form in Appendix A.

In Table 1 we show the maximal allowed number of VL fermions,  $N_{F_{\max}}$ , for which the gauge couplings remain perturbative ( $g_i \lesssim 4\pi$ ) up to  $10^{15}$  GeV. One can see that color octets and electroweak quadruplets are the highest representations possible, and that a total number of 11 different combinations of  $SU(3)_C$  and  $SU(2)_L$  charges is allowed. Non-zero hypercharge

<sup>3</sup>The impact of non-gauge interactions on unification of the gauge couplings will be discussed elsewhere.

<sup>4</sup>Note that we consider this particular value as a rough estimate of the limit imposed on the value of the GUT scale by proton decay measurement. The actual experimental bounds will be discussed in Sec. 4

can only reduce the value of  $N_{F_{\max}}$ . Thus, the requirement of perturbativity up to around the unification scale reduces the possible number of VL fermions that transform under  $SU(3)_C$  and  $SU(2)_L$ . In some cases, however,  $N_{F_{\max}}$  exceeds the maximum number of 12 VL copies adopted in Ref. [28]. We will demonstrate in Sec. 3 that several novel solutions with respect to those presented in Ref. [28] can be found if that somewhat arbitrary assumption is relaxed.

So far our discussion was quite generic as the conclusions regarding the properties of the allowed VL representations resulted merely from the requirement of perturbativity, independently on what happens at the unification scale and how the expected GUT symmetry is realized. It is, however, not the case for the hypercharge. This particular quantum number is much more difficult to deal with in a general manner, as in principle it can assume continuous values. Additionally, hypercharge normalization is not unique as it depends on a particular embedding of the SM into a GUT gauge group [39], and different normalizations may lead to different predictions regarding the gauge coupling unification. For these reasons we have to depart at this point from an entirely model-independent approach.

We assume from now on that at the unification scale the  $SU(5)$  symmetry is restored and VL fermions are embedded into multiplets of  $SU(5)$  just like it is the case for the SM fields. This seems to be the most natural choice since  $SU(5)$  not only can play the role of a self-contained unified gauge symmetry [1], but also shows up in breaking chains of larger GUT groups. In Appendix B the decomposition of the irreducible  $SU(5)$  representations of increasing dimensions into irreducible representations of the SM gauge group is summarized. It is enough to consider representations up to dimension 75, since the larger ones decompose either to representations that have already appeared in Eq. 30, or to representations whose dimensions exceed the limits presented in Table 1. Additionally, in Table 2 we provide information about the maximal value of hypercharge for a single pair of VL fermions ( $N_F = 2$ ), for which the gauge couplings remain perturbative up to  $10^{15}$  GeV. When combined, perturbativity bounds in Tables 1 and 2 eliminate some of representations listed in Eq. 30. Eventually, we are left with a set of 24 distinct non-singlet  $SU(3)_C \times SU(2)_L \times U(1)_Y$  representations:

$$\begin{aligned}
\text{color singlets : } & (\mathbf{1}, \mathbf{1}, 1), (\mathbf{1}, \mathbf{1}, -2), (\mathbf{1}, \mathbf{2}, \frac{1}{2}), (\mathbf{1}, \mathbf{2}, -\frac{3}{2}), (\mathbf{1}, \mathbf{3}, 0), (\mathbf{1}, \mathbf{3}, 1), & (3) \\
& (\mathbf{1}, \mathbf{4}, \frac{1}{2}), (\mathbf{1}, \mathbf{4}, -\frac{3}{2}), \\
\text{color triplets : } & (\mathbf{3}, \mathbf{1}, -\frac{1}{3}), (\bar{\mathbf{3}}, \mathbf{1}, -\frac{2}{3}), (\bar{\mathbf{3}}, \mathbf{1}, \frac{4}{3}), (\bar{\mathbf{3}}, \mathbf{1}, -\frac{5}{3}), (\mathbf{3}, \mathbf{2}, \frac{1}{6}), (\bar{\mathbf{3}}, \mathbf{2}, \frac{5}{6}), \\
& (\bar{\mathbf{3}}, \mathbf{2}, -\frac{7}{6}), (\mathbf{3}, \mathbf{3}, -\frac{1}{3}), (\bar{\mathbf{3}}, \mathbf{3}, -\frac{2}{3}), \\
\text{color sextets : } & (\bar{\mathbf{6}}, \mathbf{1}, -\frac{1}{3}), (\mathbf{6}, \mathbf{1}, -\frac{2}{3}), (\bar{\mathbf{6}}, \mathbf{2}, \frac{1}{6}), (\mathbf{6}, \mathbf{2}, \frac{5}{6}), \\
\text{color octets : } & (\mathbf{8}, \mathbf{1}, 0), (\mathbf{8}, \mathbf{1}, 1), (\mathbf{8}, \mathbf{2}, \frac{1}{2}).
\end{aligned}$$

These are the fundamental building blocks of the VL unification scenarios we are going to analyze in the next section.

### 3 VL models with precise gauge unification

We are now in the position to perform a comprehensive analysis of the SM extensions with VL fermions that could potentially lead to precise unification of three SM gauge couplings at the energies in the range  $[10^{15} - 10^{18}]$  GeV. With this goal in mind, we would like

to proceed in a systematic way, gradually increasing the complexity of the constructed models. The simplest scenarios could be engineered by adding to the SM one of the VL representations listed in Eq. 3. It is, however, a known fact [28] that precise unification is not possible within such a framework. The next possibility is then to consider two different VL representations with an arbitrary number of fermion copies within each of them. Theoretical and phenomenological properties of such models are the main objective of the present study.

Adding three (or more) independent VL representations makes our task more and more challenging. Note that 276 distinctive combinations of the VL representations listed in Eq. 3 need to be considered in the two-representation case. This figure increases to 2024 when three, and to 10626 when four different representations are considered. Each combination requires to scan over the numbers of VL fermions in each representation (see Table 1), as well as on their masses, which we always assume to be uncorrelated. This means that numerical complexity of the problem grows exponentially with every independent representation added. For this reason we focus in this study on the simplest case, leaving more complicated SM extensions for future work.

The numerical procedure employed in our analysis is the following. We use the 2-loop SM RGEs from  $M_t$  up to the scale  $M_1$ , at which the lightest of VL fermions show up in the spectrum. We assume for simplicity that all  $N_F$  copies of the same representation have a common mass. Above  $M_1$  we switch to the 2-loop RGEs for a generic BSM scenario, Eq. 15-17. At the scale  $M_2$  the effects of heavier VL fermions need to be taken into account. Finally, we define a unification scale,  $M_{\text{GUT}}$ , as the scale at which all three gauge couplings acquire a common value,  $g_{\text{GUT}}$ ,

$$g_{\text{GUT}} = g_3(M_{\text{GUT}}) = g_2(M_{\text{GUT}}) = g_1(M_{\text{GUT}}). \quad (4)$$

We require that the unified coupling is perturbative, i.e.  $g_{\text{GUT}} \leq 4\pi$ .

Precision of the gauge coupling unification can be quantified by a set of three mismatch parameters,  $\epsilon_{1,2,3}$ . For each combinations  $(i, j)$ , where  $i, j = 1, 2, 3$ , we determine a two coupling unification scale from the condition  $g_i(M_{\text{GUT}}^{ij}) = g_j(M_{\text{GUT}}^{ij}) = g_{ij}$ . We then define a deviation of the third coupling from  $g_{ij}$  as

$$\epsilon_k = \frac{g_k^2(M_{\text{GUT}}^{ij}) - g_{ij}^2}{g_{ij}^2} \quad (5)$$

and determine the true unification scale by requiring  $\epsilon_{\text{GUT}} = \min(\epsilon_1, \epsilon_2, \epsilon_3)$ . In the SM  $\epsilon_{\text{GUT}}^{\text{SM}} = 7.3\%$ , indicating that the running values of the three gauge couplings do not really converge to a common number. On the other hand, in the minimal SUSY version of the SM, which is a benchmark BSM scenario for the gauge coupling unification,  $\epsilon_{\text{GUT}}^{\text{MSSM}} = 1.1\%$  when all sparticle masses set at 1 TeV. Therefore, we define the *precise gauge unification* (PGU) by a condition  $\epsilon < 1\%$ .

For each of 276 scenarios with two distinctive VL representations we scan over the number of BSM fermions,  $N_1, N_2$ , and their masses,  $M_1, M_2$ , and for each point in the 4-dimensional parameter space we determine  $\epsilon_{\text{GUT}}$  and  $M_{\text{GUT}}$ . The parameters  $M_1$  and  $M_2$  are varied between 0.25 TeV and 10 TeV. The main results of the analyses are summarized in Table 3. We found 13 different scenarios that allow for the PGU at the scale  $10^{15} - 10^{18}$  GeV. Nine of them have been previously identified in [28], while the scenarios F2, F3, F6 and F13 present

Scenario	$\mathbf{R}_{F_1}$	$\mathbf{R}_{F_2}$	$N_1$	$N_2$	VL mass/GUT scale
F1	$(\mathbf{1}, \mathbf{2}, \frac{1}{2})$	$(\mathbf{6}, \mathbf{1}, \frac{1}{3})$	12	2	Fig. 1(a)
F2	$(\mathbf{1}, \mathbf{2}, \frac{1}{2})$	$(\mathbf{6}, \mathbf{1}, \frac{1}{3})$	20	4	Fig. 1(b)
F3	$(\mathbf{1}, \mathbf{2}, \frac{1}{2})$	$(\mathbf{6}, \mathbf{1}, \frac{1}{3})$	22	4	Fig. 1(c)
F4	$(\mathbf{1}, \mathbf{2}, \frac{1}{2})$	$(\mathbf{8}, \mathbf{1}, 0)$	8	1	Fig. 1(d)
F5	$(\mathbf{1}, \mathbf{2}, \frac{1}{2})$	$(\mathbf{8}, \mathbf{1}, 0)$	12	2	Fig. 1(e)
F6	$(\mathbf{1}, \mathbf{2}, \frac{1}{2})$	$(\mathbf{8}, \mathbf{1}, 0)$	14	2	Fig. 1(f)
F7	$(\mathbf{1}, \mathbf{3}, 0)$	$(\mathbf{3}, \mathbf{1}, -\frac{1}{3})$	2	8	Fig. 1(g)
F8	$(\mathbf{1}, \mathbf{3}, 0)$	$(\mathbf{3}, \mathbf{1}, -\frac{1}{3})$	3	12	Fig. 1(h)
F9	$(\mathbf{1}, \mathbf{3}, 0)$	$(\mathbf{6}, \mathbf{1}, -\frac{2}{3})$	3	2	Fig. 1(i)
F10	$(\mathbf{1}, \mathbf{4}, \frac{1}{2})$	$(\mathbf{6}, \mathbf{1}, -\frac{2}{3})$	2	4	Fig. 2(a)
F11	$(\mathbf{3}, \mathbf{1}, -\frac{1}{3})$	$(\mathbf{3}, \mathbf{2}, \frac{1}{6})$	2	2	Fig. 2(b)
F12	$(\mathbf{3}, \mathbf{1}, \frac{2}{3})$	$(\mathbf{3}, \mathbf{2}, \frac{1}{6})$	4	4	Fig. 2(c)
F13	$(\mathbf{3}, \mathbf{1}, \frac{2}{3})$	$(\mathbf{3}, \mathbf{2}, \frac{1}{6})$	6	6	Fig. 2(d)

Table 3: Scenarios with 2 representations of VL fermions that allow for the PGU ( $\epsilon_{\text{GUT}} \leq 1\%$ ) and the associated unification scale lies in the range  $10^{15} - 10^{18}$  GeV. The VL masses vary between 0.25 TeV and 10 TeV. In columns 2 and 3 transformation properties of both representations with respect to the SM gauge symmetry group are given. It is understood that, if applicable,  $\mathbf{R}_F$  also encompasses its own complex conjugation. Columns 4 and 5 display number of VL fermions in each representation. In the last column we direct the reader to a corresponding figure illustrating the allowed VL mass ranges and the iso-contours of the unification scale.

completely novel solutions, characterized by either more than 12 copies of VL fermions in one of the representations, or VL masses larger than 5 TeV. Note that some of the successful combinations of representations allow for various choices of fermion numbers. This is, for example, the case for the scenarios F1, F2 and F3, in which VL fields transforming as  $(\mathbf{1}, \mathbf{2}, \frac{1}{2})$  and  $(\mathbf{1}, \bar{\mathbf{2}}, -\frac{1}{2})$  of  $SU(3)_C \times SU(2)_L \times U(1)_Y$  can show up in 12, 20 and 22 copies, while those transforming as  $(\mathbf{6}, \mathbf{1}, \frac{1}{3})$  and  $(\bar{\mathbf{6}}, \mathbf{1}, -\frac{1}{3})$  in 2 and 4 copies. Thus, only 7 combinations of  $R_3$  and  $R_2$  are really unique.

Among 24 various representations listed in Eq. 3, only 9 can contribute to the successful unification. These are adjoint representations of both  $SU(3)_C$  and  $SU(2)_L$  gauge groups,  $(\mathbf{8}, \mathbf{1}, 0)$  and  $(\mathbf{1}, \mathbf{3}, 0)$ ; fundamental representations under which the SM left-handed quarks and leptons transform,  $(\mathbf{3}, \mathbf{2}, \frac{1}{6})$  and  $(\mathbf{1}, \mathbf{2}, \frac{1}{2})$ ; fundamental representations of the SM right-handed up and down quarks,  $(\mathbf{3}, \mathbf{1}, -\frac{2}{3})$ ,  $(\mathbf{3}, \mathbf{1}, -\frac{1}{3})$ ; and three exotic representations that are not realized by the ordinary matter. Incidentally, the resemblance of the quantum numbers characterizing VL fermions that allow for the PGU to the ones of the SM particles can have important phenomenological consequences once the Yukawa-driven mixing with the SM fermions is allowed.

It turns out that whether the gauge coupling unification is possible in a given model hinges strongly on hierarchy among the VL fermion masses. To illustrate this dependence, in Fig. 1 and Fig. 2 we present a distribution of the mismatch parameter  $\epsilon_{\text{GUT}}$  as a function of  $M_1$  and  $M_2$  for all 13 scenarios summarized in Table 3. In red the region of the PGU is indicated, which will be of main interest for our further phenomenological analysis. As an additional information, we show in different shades of yellow departure from the precise

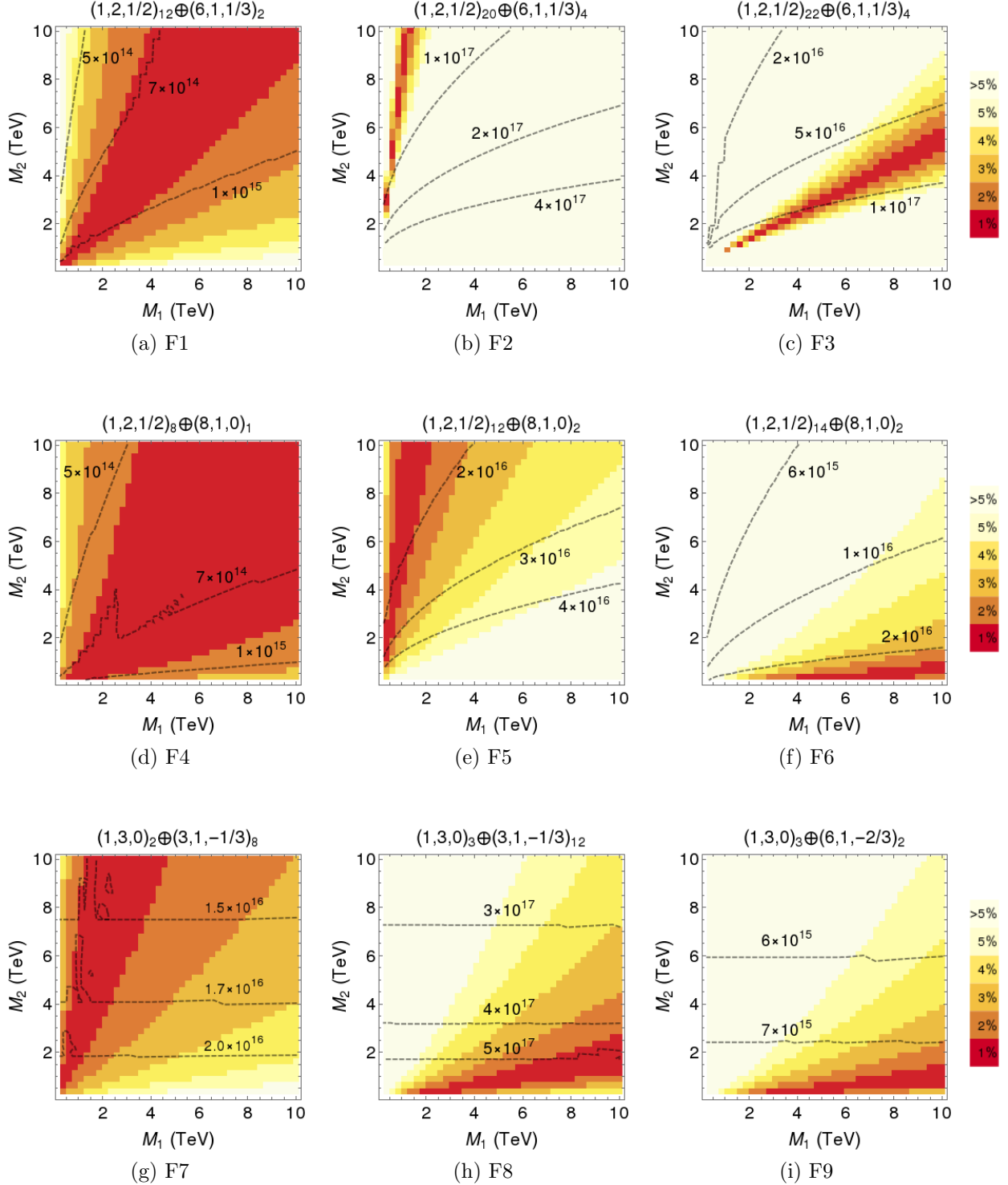


Figure 1: Distribution of the mismatch parameter  $\epsilon_{\text{GUT}}$  as a function of  $M_1$  and  $M_2$  for the scenarios F1 - F9 of Table 3. Red area corresponds to the PGU ( $\epsilon_{\text{GUT}} \leq 1\%$ ). Different shades of yellow illustrate departure from the precise unification condition as quantified by the increasing values of  $\epsilon_{\text{GUT}}$ . Isocontours of the unification scale (in GeV) are indicated as dashed black curves.



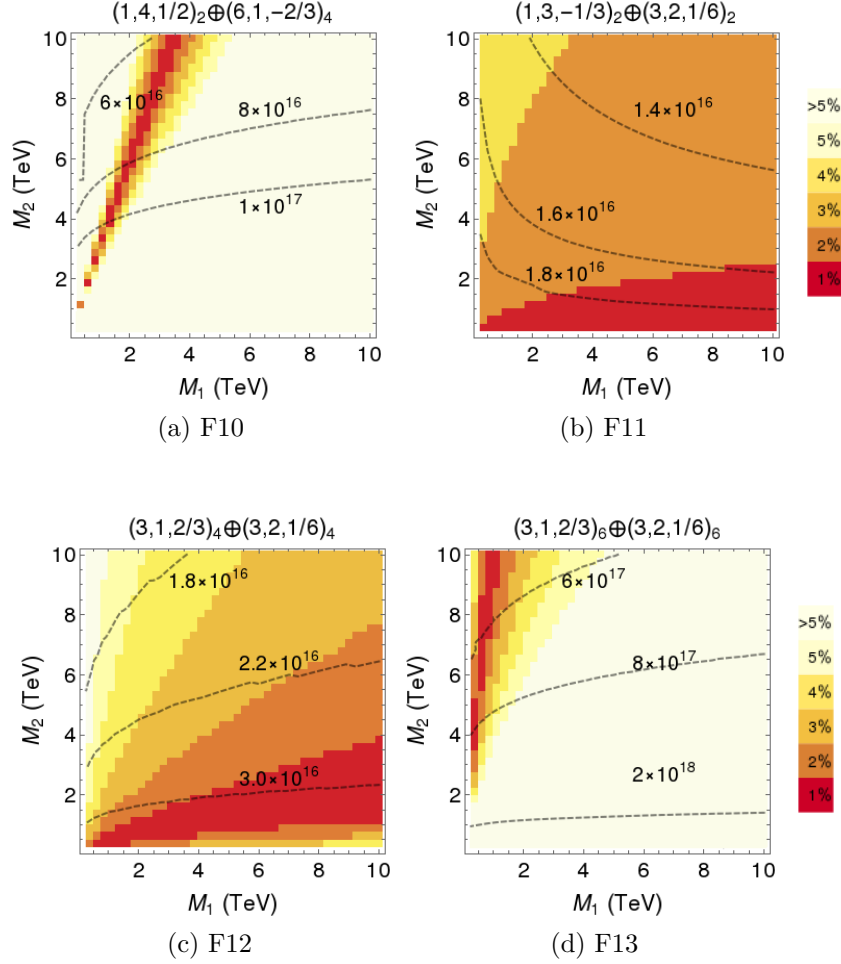


Figure 2: Distribution of the mismatch parameter  $\epsilon_{\text{GUT}}$  as a function of  $M_1$  and  $M_2$  for the scenarios F10 - F13 of Table 3. Red area corresponds to the PGU ( $\epsilon_{\text{GUT}} \leq 1\%$ ). Different shades of yellow illustrate departure from the precise unification condition as quantified by the increasing values of  $\epsilon_{\text{GUT}}$ . Isocontours of the unification scale (in GeV) are indicated as dashed black curves.

unification condition as quantified by the increasing values of  $\epsilon_{\text{GUT}}$ . The width of the color bands can give one some idea on how easy the unification is, or, in other words, what is the required degree of fine-tuning among the mass parameters.

The successful PGU scenarios can be divided in three distinctive categories, depending on the required mass hierarchy among the VL fermions. We will be referring to them later using the following labels:

$$\begin{aligned}
 \text{H0} : M_1 &\sim M_2, & \text{scenarios } &\text{F1, F3, F4,} & (6) \\
 \text{H1} : M_1 &\gg M_2, & \text{scenarios } &\text{F6, F8, F9, F11, F12,} \\
 \text{H2} : M_1 &\ll M_2, & \text{scenarios } &\text{F2, F5, F7, F10, F13.}
 \end{aligned}$$

In Sec. 4 we will demonstrate that the mass hierarchy characterizing a given scenario is crucial for the way the scenario can be tested experimentally.

Another quantity that significantly differentiates among the VL combinations listed in

	Low	Medium	High
H0	<b>F1, F4</b>		<b>F3</b>
H1	<b>F9</b>	<b>F6, F11</b> <b>F12</b>	<b>F8</b>
H2		<b>F2, F5</b> <b>F7, F10</b>	<b>F13</b>

Table 4: Properties of the PGU scenarios in terms of the VL mass hierarchy and the unification scale and their susceptibility to various experimental search strategies. Light blue indicates the models that are tested by the proton decay measurements. Those highlighted in light green can be subject to color searches:  $R$ -hadrons and running of the strong gauge coupling. Light red corresponds to the scenarios tested through EW interaction in lepton-like HSCP searches and EW precision tests.

Table 3 is the unification scale. In Fig. 1 and Fig. 2 its isocontours are indicated as dashed black curves. Depending on the order of magnitude of  $M_{\text{GUT}}$ , we divide our scenarios in three categories:

$$\begin{aligned}
\text{Low} : M_{\text{GUT}} &\simeq 10^{15} \text{ GeV}, & \text{scenarios } & \text{F1, F4, F9}, \\
\text{Medium} : M_{\text{GUT}} &\sim 10^{16} \text{ GeV}, & \text{scenarios } & \text{F2, F5, F6, F7, F10, F11, F12}, \\
\text{High} : M_{\text{GUT}} &\sim 10^{17} \text{ GeV}, & \text{scenarios } & \text{F3, F8, F13}.
\end{aligned} \tag{7}$$

We summarize the characteristics of the PGU scenarios in terms of the VL mass hierarchy and the unification scale in Table 4. The color code refers to experimental techniques that can be employed in order to test the available parameter space of a model. We will discuss them in details in Sec. 4.

Before closing this section, we would like to comment on the fate of the identified PGU scenarios when the VL masses are pushed to energies much higher than 10 TeV. To analyze this issue, we repeated the numerical procedure of Sec. 3 extending the scanning ranges of  $M_1$  and  $M_2$  up to  $10^{10}$  TeV. We found that all the models listed in Table 3, except F1 and F4, remain valid at higher energies, as could be anticipated from the shape of the red areas in Fig. 1 and Fig. 2. Additionally, several new combinations of two VL representations become available.

The high energy behavior of the PGU scenarios may seem somehow discouraging, as in principle one may put the VL fermions well above the reach of any existing collider experiment and still achieve the gauge coupling unification. There is, however, one important remark to be made. The main factor that decides whether a given scenario is accepted or not, is the value of the unification scale, which we require to stay in the range  $10^{15} - 10^{18}$  GeV. When the mass of VL fermions increases, the unification scale decreases, as confirmed by the shape of  $M_{\text{GUT}}$  isocontours in Fig. 1 and Fig. 2. As a consequence, experimental bounds from the proton decay measurements may at some point come into play. In the next section we will show that this is indeed the case and that the allowed parameter space of the PGU scenarios is limited from above.

## 4 Experimental tests of the PGU scenarios

In the previous section we identified all possible combinations of two VL fermion representations that allow for precise unification of the three SM gauge couplings. In the following we will focus on phenomenological properties of the PGU scenarios and discuss in details various experimental ways of testing the available parameter space. We remind the reader that we assume negligible Yukawa couplings among the BSM sector and the SM, therefore our VL fermions can only be produced via gauge interactions. Experimental signatures of the models with a large number of VL fermions have been discussed by one of us in Ref. [40] and we follow closely its approach. We will demonstrate the complementarity among the bounds provided by various experimental searches, resulting from the fact that each of them aim at constraining particular sets of color and electroweak quantum numbers. In combination with the specific mass hierarchies required by the PGU (see Table 4), it will allow us to derive strong lower bounds on the VL masses.

### 4.1 Proton decay

We assume that at the unification scale the symmetry group  $SU(3)_C \times SU(2)_L \times U(1)_Y$  is embedded into a larger GUT group. Since in the unified framework the SM quarks and leptons belong to the same GUT multiplets, interactions are generated, mediated by heavy gauge bosons, that violate both the baryon and lepton number conservation. Proton decay is then a generic prediction of such scenarios. In non-SUSY models the dominant contribution to the proton decay width comes from dimension-6 gauge operators of the common structure  $QQQL$ . The exact form of these contributions highly depends on the realization of the GUT symmetry. However, a rough estimation of the proton lifetime can be made [41]

$$\tau_p = \left( \frac{4\pi}{g_{\text{GUT}}^2} \right)^2 \left( \frac{M_{\text{GUT}}}{\text{GeV}} \right)^4 \times 2.0 \times 10^{-32} \text{ years}, \quad (8)$$

as a simple function of the unification scale  $M_{\text{GUT}}$  and the value of the unified gauge coupling  $g_{\text{GUT}}$ .

Proton decay has been experimentally searched for since the early 1990s by Super-Kamiokande (SK) underground water Cherenkov detector. The strongest lower bound on the proton lifetime is set by the decay channel  $p \rightarrow e^+ \pi^0$  and reads  $\tau_p > 1.6 \times 10^{34}$  years [42]. Hyper-Kamiokande (HK), a next generation machine, will be able to extend the limit by at least one order of magnitude, up to  $\sim 2 \times 10^{35}$  years [43].

The present (solid blue line) and projected (dashed blue line) limits from the proton decay as a function of the VL masses  $M_1$  and  $M_2$  are shown in Figs. 3 and 4. The shaded blue area above the lines is disfavored. Scenarios F1 and F4 are already entirely excluded by the SK measurements. Scenario F9, on the other hand, is going to be entirely tested by HK. Scenarios that fall within the reach of the current proton decay experiments are also marked in Table 4 in light blue. As expected, all of them belong to the category “low unification scale”.

Proton decay provides a unique experimental way of testing the PGU scenarios characterized by the BSM sector at the energy scales far above the reach of any present-day collider experiment. In fact, for all but one models from Table 3 it provides upper bounds on

Model	Proton decay		Running $g_3$		$R$ -hadrons		HSCP		EWPO		Summary plot
	$M_1^{\max}$	$M_2^{\max}$	$M_1^{\min}$	$M_2^{\min}$	$M_1^{\min}$	$M_2^{\min}$	$M_1^{\min}$	$M_2^{\min}$	$M_1^{\min}$	$M_2^{\min}$	
F1	Excluded		-	0.7	-	1.8	0.8	-	1.7	-	Fig. 3(a)
F2	25	180	-	1.1	-	1.8	0.8	(6.0)	2.0	-	Fig. 3(b)
F3	350	200	-	1.1	(2.2)	1.8	0.8	-	2.2	-	Fig. 3(c)
F4	Excluded		-	0.4	(1.2)	2.0	0.8	-	1.2	-	Fig. 3(d)
F5	10	50	-	0.8	-	2.0	0.8	(3.0)	1.5	-	Fig. 3(e)
F6	500	50	(9.0)	0.8	(>10)	2.0	0.8	-	1.7	-	Fig. 3(f)
F7	20	100	-	0.5	-	1.7	1.1	-	1.2	-	Fig. 3(g)
F8	$2 \times 10^5$	$5 \times 10^5$	(3.0)	0.8	(6.0)	1.7	1.1	-	1.2	-	Fig. 3(h)
F9	Excluded HK		(4.5)	0.7	(>10)	1.8	1.1	-	1.5	-	Fig. 3(i)
F10	250	1000	-	1.1	-	1.8	1.2	(3.0)	2.0	-	Fig. 4(a)
F11	600	200	0.2	0.2	(5.0)	1.8	-	-	0.5	1.0	Fig. 4(b)
F12	$6 \times 10^4$	400	0.2	0.6	(4.0)	1.8	-	-	0.7	1.5	Fig. 4(c)
F13	-	$2 \times 10^6$	0.5	0.8	1.7	(>10)	-	-	0.7	1.7	Fig. 4(d)

Table 5: Exclusion bounds on the VL masses  $M_1$  and  $M_2$  provided by different experiments (all in TeV). In column 2 we indicate the models that are excluded by the measurement of the proton lifetime by Super-Kamiokande [42], as well as the upper bounds provided by the projected Hyper-Kamiokande measurement [43]. In column 3 limits from the running strong coupling constant measurement by CMS [44] are shown. The numbers in parentheses indicate indirect limits whose derivation is described in the text. In columns 4 and 5 bounds from the ATLAS 13 TeV HSCP searches [45] are presented, for colored and non-colored particles, respectively. 100 TeV projections for the EWP tests [46] are shown in column 6.

the allowed VL masses. We report them in the second column of Table 5 for the projected reach from HK (the corresponding current bounds from SK are approximately one order of magnitude weaker). One can see that for several scenarios that belong to the medium GUT-scale category the upper bounds on VL masses are of the order of “only” several-tens TeV. This feature opens up an exiting possibility of entirely probing those scenarios in the (however distant) future.

## 4.2 Running of the strong gauge coupling

The RG running of the strong gauge coupling constant has been tested experimentally up to the energies of around 1.5 TeV. The most recent data comes from the measurement of double-differential inclusive jet cross section at  $\sqrt{s} = 8$  TeV with an integrated luminosity of 19.6/fb by the CMS Collaboration [44]. The value of the running coupling is extracted from the data as a function of the energy scale at which it is evaluated. The measurement is consistent with the predictions of the SM and as such poses a constraint on the minimal mass of any exotic colored particle.

In the third column of Table 5 we summarize the lower bounds on the VL masses  $M_1$  and  $M_2$  in each PGU scenario. The same limits are also depicted in Figs. 3 and 4 as dark green solid lines. Obviously, only the representations that transform non-trivially under  $SU(3)_C$  can be directly constrained by the data.

There is, however, an interesting observation to be made. In the scenarios with the mass

hierarchy H1, characterized by the color VL fermions much lighter than the non-colored ones, the running strong coupling allows one to indirectly put very strong lower bounds on masses of the fermions that are  $SU(3)_C$  singlets and would be otherwise not affected by the CMS measurement. We indicate them in Table 5 as numbers in parentheses. As an example, let us consider scenario F6, whose parameter space is subject to various experimental constraints presented in Fig. 3(f). The direct lower bound on  $M_2$  from the running of  $g_3$  reads in this case 0.8 TeV. The PGU region, however, is located in the lower part of the plot, as the unification requirement imposes  $M_1 \gg M_2$ . As a result, it is almost entirely probed by CMS and an indirect bound on the mass  $M_1$  can be derived, which reads in this case  $M_1 \gtrsim 9$  TeV. We will later see that the indirect limits from the running of the strong coupling constant are actually stronger than any other bound provided by dedicated electroweak searches.

Enhanced susceptibility to color searches is marked in Table 4 in light green and, as explained above, it corresponds to the mass hierarchy H1. It is yet another example of the complementarity among particular properties of the PGU scenarios and their testability.

### 4.3 Direct LHC searches

In the absence of Yukawa interactions with the SM quarks and leptons, the VL fermions are stable<sup>5</sup> and can be experimentally looked for at colliders through heavy stable charged particle (HSCP) searches. Dedicated analyses performed both by the ATLAS and CMS collaborations utilize observables related to the ionization energy loss ( $dE/dx$ ) and time of flight (ToF), which allow to distinguish massive and non-relativistic HS CPs from the light SM particles traveling with velocities close to the speed of light.

Two categories of signals are usually considered, depending on the type of charges carried by HSCP: one that consists of particles interacting strongly, and another in which HS CPs are lepton-like color singlets. The two would differ both by the production mechanism at the LHC and by the size of the production cross section. In the following we will discuss them separately.

#### 4.3.1 Colored HSCP

Let us first assume that a heavy stable particle can interact strongly. If the lifetime of such a colored HSCP is longer than typical hadronization time scale, it can form colorless QCD bound states with the SM quarks and gluons, the so-called  $R$ -hadrons.

The most recent ToF and  $dE/dx$  based analyses have been performed by ATLAS using a data sample corresponding to  $36 \text{ fb}^{-1}$  of proton-proton collisions at  $\sqrt{s} = 13$  TeV [45], and by CMS using  $2.5 \text{ fb}^{-1}$  of data at the same energy [47]. Since in both cases no significant deviations from the expected SM background have been observed, a model-independent 95% confidence level (C.L.) upper bound on the  $R$ -hadron production cross section can be derived.

---

<sup>5</sup>The presence of a stable charged particle at cosmological scales may be problematic from the point of view of dark matter properties. A way out is to introduce Yukawa interaction with the SM, small enough not to affect the RG running but large enough to allow the charged particle to decay. Note, however, that in the case of representations  $(\mathbf{8}, \mathbf{1}, 0)$ ,  $(\mathbf{6}, \mathbf{1}, \frac{1}{3})$  and  $(\mathbf{6}, \mathbf{1}, \frac{2}{3})$  it is not possible to construct a decay operator with the SM matter. One would need to introduce, for example, additional scalars charged under  $SU(3)_C$ . This provides a motivation to extend the current analyses in the future to include the scalar fields.

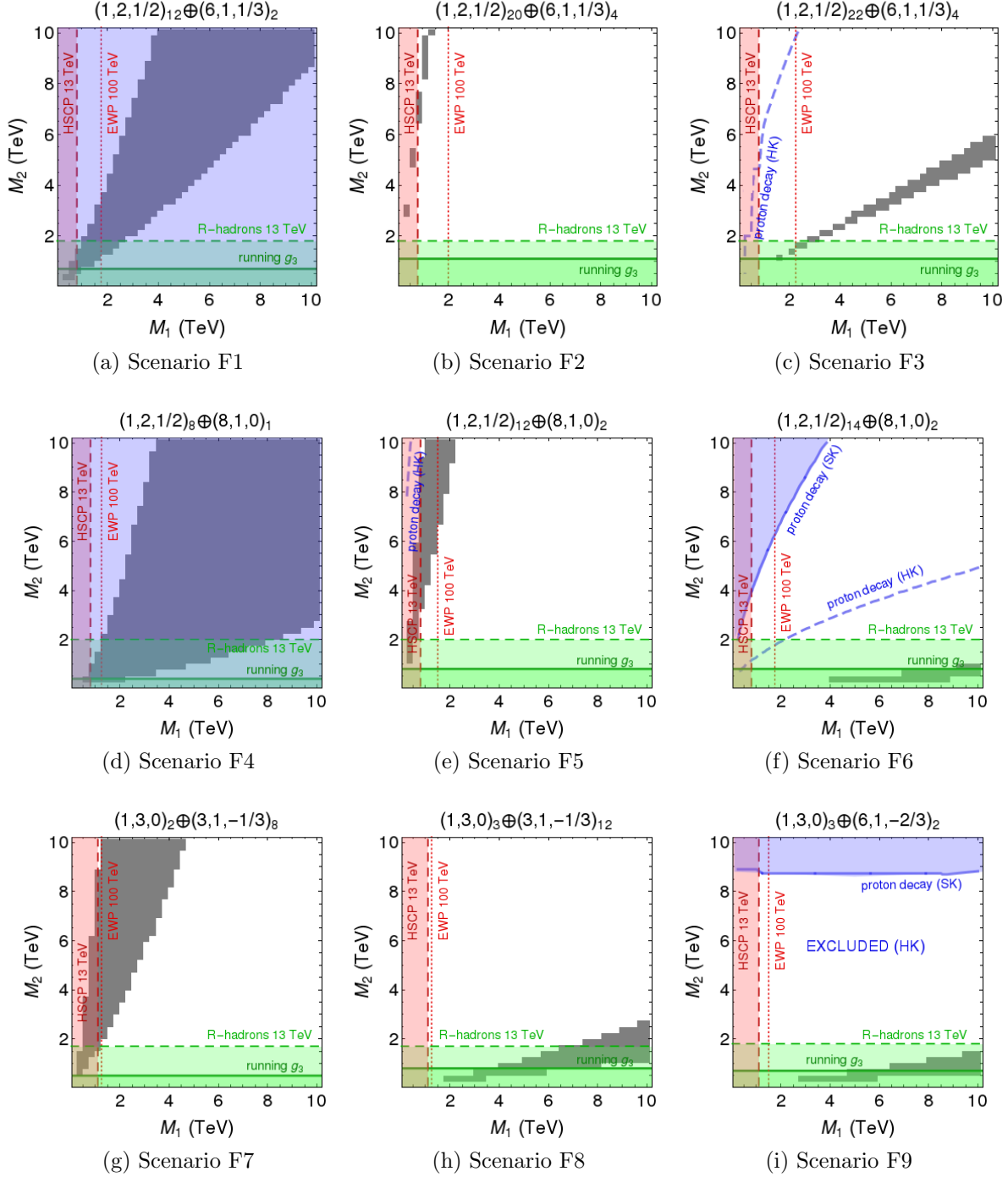


Figure 3: Summary of experimental bounds on VL masses  $M_1$  and  $M_2$  for scenarios F1-F9. In gray the PGU region is indicated. The area below and left to the solid green line is excluded by the measurement of the running strong coupling constant by CMS [44]. The limits from the 13 TeV ATLAS  $R$ -hadrons search [45] are indicated as a dashed green line. The corresponding lepton-like HSCP search excludes the area left to the dashed red line. 100 TeV projections for the EWP tests [46] are depicted as red dotted lines. Blue shaded region marks the exclusion by the proton decay measurement at Super-Kamiokande [42]. A projected reach of Hyper-Kamiokande [43] is shown as a blue dashed line.

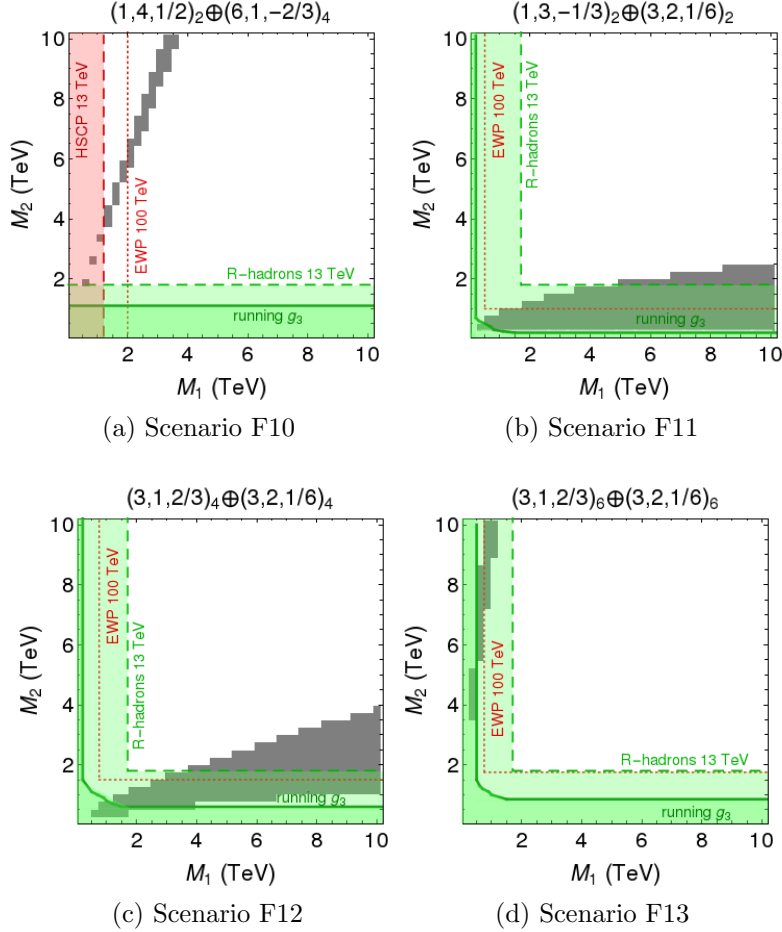


Figure 4: The same as Fig. 3 but for scenarios F10-F13.

Such a result can then be translated into a lower bound on the BSM fermion mass within an arbitrary framework. An example usually considered by the collaborations is the gluino, the SUSY partner of the gluon and a benchmark for a BSM fermion with the SM charges  $(\mathbf{8}, \mathbf{1}, 0)$ . The lower bound on the long-lived gluino mass reads 1.5 TeV for CMS and 2.0 TeV for ATLAS.

In hadron colliders, any colored BSM fermion would be pair-produced at the leading order through gluon fusion or by quark-antiquark annihilation, with the production cross section that solely depends on the  $SU(3)_C$  quantum numbers. We calculated the  $pp \rightarrow \bar{Q}Q$  cross section at the leading order (LO) using `MadGraph5_aMC@NLO`, and then rescaled it with the  $k$ -factor of 2 [48] to account for higher-order QCD corrections and to reproduce the cross section quoted in [45] for gluino pair-production.<sup>6</sup> We then compared the result with the observed exclusion limit on the gluino derived by ATLAS. The corresponding exclusion bounds applied to parameters  $M_1$  and  $M_2$  are indicated in Figs. 3 and 4 as dashed green lines. We also summarize them in the fourth column of Table 5.

<sup>6</sup>The cross section changes by over three orders of magnitude over the VL mass range considered in [45]. The resulting exclusion bound is, therefore, very mildly sensitive to higher-order order corrections to the cross section.

The limits from the  $R$ -hadron searches probe the parameter space in the same direction as the measurement of the running strong coupling constant from Sec. 4.2. Therefore, the mass parameter of the colored VL representations is constrained. As before, indirect bounds on the non-colored representations can be derived in the case of the type H1 mass hierarchy. The effect is particularly visible for scenarios F6 and F9, which turn out to be excluded by the  $R$ -hadron searches up to at least 10 TeV. In several other scenarios  $M_1$  receives a strong lower bound as well, which we indicate in Table 5 as a number in parentheses.

Note that in the presence of non-zero Yukawa interactions the VL colored fermions may decay before a bound state is formed. In such a case, the limits from the  $R$ -hadron searches will no longer apply. For that reason we indicate them in Figs. 3 and 4 with dashed lines, as contrasted with the running strong coupling constraints that are model-independent once the  $SU(3)_C$  charges are fixed.

### 4.3.2 Lepton-like HSCP

If a charged HSCP does not interact hadronically, it will be produced through Drell-Yan (DY) processes and will predominantly lose energy via ionization inside the detector. In the analysis [45] with  $36 \text{ fb}^{-1}$  of data ATLAS interpreted the model-independent results in a benchmark model that assumes DY production of charginos. The corresponding lower limits on the HSCP mass reads 1090 GeV. In the analogous study by CMS [47] based on  $2.5 \text{ fb}^{-1}$  dataset, bounds on the mass of a generic lepton-like fermions with a unit electric charge were derived at 550 GeV.

To set lower bounds on the masses of VL fermions that are  $SU(3)_C$  singlets, we used the chargino-dedicated search by ATLAS. The LO production cross sections were calculated with `MadGraph5_aMC@NLO`, but no  $k$ -factor was added. The corresponding exclusion bounds in the  $(M_1, M_2)$  plane are depicted in Figs. 3 and 4 as dashed red lines. We also summarize them in the fifth column of Table 5.

The limits from the lepton-like HSCP searches allow to probe the scenarios with the mass hierarchy H2, in which the non-colored VL fermions are lighter than the colored ones. Enhanced susceptibility to electroweak searches is marked in Table 4 in light red. In general, the limits are significantly weaker than the corresponding color-based bounds due to the lower production cross section. On the other hand, indirect lower bounds on the mass  $M_2$  can be derived in scenarios F2, F5, F10, which turns out to be much stronger than the direct bounds from the  $R$ -hadron searches or the running strong coupling measurement.

## 4.4 Electroweak precision tests

A complementary way to study properties of the VL fermions is to look at the processes below the  $M_{\text{VL}}$  mass threshold. Such an approach can result particularly important if VL fermions are too heavy to be directly produced in the colliders, or not long-lived enough for dedicated HSCP searches to be effective. In this regard, high-energy measurements of DY processes at the LHC offer a promising way to indirectly look for VL fermions by testing departures from the SM predictions in electroweak precision (EWP) observables [46].

In the VL extensions of the SM considered in this paper, the BSM contributions can manifest themselves in two oblique parameters [49, 50] that are sensitive to the presence of



Scenario	Current status	Experimental test
F1	Excluded	proton decay
F2	$M_1 > 0.8 \text{ GeV}, M_2 > 6.0 \text{ GeV}$	HSCP
F3	$M_1 > 2.2 \text{ GeV}, M_2 > 1.8 \text{ GeV}$	$R$ -hadrons
F4	Excluded	proton decay
F5	$M_1 > 0.8 \text{ GeV}, M_2 > 3.0 \text{ GeV}$	HSCP
F6	Excluded up to 10 TeV	$R$ -hadrons
F7	$M_1 > 1.1 \text{ GeV}, M_2 > 1.7 \text{ GeV}$	$R$ -hadrons, HSCP
F8	$M_1 > 6.0 \text{ GeV}, M_2 > 1.7 \text{ GeV}$	$R$ -hadrons
F9	To be tested by HK	proton decay
F10	$M_1 > 1.2 \text{ GeV}, M_2 > 3.0 \text{ GeV}$	HSCP
F11	$M_1 > 5.0 \text{ GeV}, M_2 > 1.8 \text{ GeV}$	$R$ -hadrons
F12	$M_1 > 4.0 \text{ GeV}, M_2 > 1.8 \text{ GeV}$	$R$ -hadrons
F13	Excluded up to 10 TeV	$R$ -hadrons

Table 6: Summary of current experimental status of the successful PGU scenarios.

states charged under the EW gauge symmetry,  $W$  and  $Y$ . The experimental bounds on  $W$  and  $Y$  are derived from the measurements of charged and neutral currents DY at hadron colliders. The VL fermion contributions to the parameters  $W$  and  $Y$  are directly related to the corresponding beta functions and given by [51]

$$W, Y = \frac{g_{2,1}^2}{80\pi^2} \frac{m_W^2}{M_{\text{VL}}^2} \times \Delta B_{2,1}^{\text{BSM}}. \quad (9)$$

Here,  $\Delta B_{2,1}^{\text{BSM}}$  denote the pure BSM contributions to the one-loop coefficients  $B_{2,1}$ , Eq. 19 and Eq. 20, respectively.

The most up-to-date EWP experimental limits have been presented in [46], including data from LEP [52] and LHC 8 TeV measurements by ATLAS [53] and CMS [54]. We checked that they do not provide any bounds on the parameter space of the PGU scenarios under study. However, since the effects of  $W$  and  $Y$  on DY processes grow with energy, the present experimental bounds can be significantly improved at the future colliders, by roughly two orders of magnitude at the projected 100 TeV machine [46]. The corresponding projections with  $3 \text{ ab}^{-1}$  are depicted in Figs. 3 and 4 as dotted red lines. They are also summarized in the sixth column of Table 5.

As expected from the size of the corresponding gauge couplings and group-theoretical factors, the constraints on  $W$  are stronger than those on  $Y$ . Therefore, the projected EWP bounds are particularly powerful for VL representations with the non-trivial  $SU(2)_L$  charges. As a consequence, in most cases it is the mass parameter  $M_1$  that can be directly constrained by the EWP tests. The only exceptions are scenarios F11-F13, in which both VL representations can be constrained. Note also that in those three cases the projected EWP bounds can actually be competitive with the present day measurement of the running strong gauge coupling constant. Finally, it is worth to stress that similarly to what we observed in Sec. 4.3.2 for the lepton-like HSCP searches, in the PGU scenarios with the mass hierarchy H2 indirect lower bounds on the mass of the  $SU(2)_L$  singlet representations  $M_2$  can be obtained.

To summarize the findings of this section, we collect in Table 6 information about the current experimental status of the successful PGU scenarios. In this regards, we can divide them into three distinct categories. The first one encompasses scenarios F1 and F4, which are already excluded by the proton decay measurements, and scenario F9, which will be entirely tested by Hyper-Kamiokande. The second category corresponds to those scenarios (F6 and F13) that are excluded up to at least 10 TeV, but which become allowed once higher VL masses are considered. The remaining eight scenarios feature the parameter space that still evades experimental bounds for VL masses in the multi- TeV regime. It should be noted, however, that some of them (F2, F5, F8 and F11) could be in the future and with more data entirely tested within the considered mass range by the HSCP searches, while two others (F7 and F12) can be tested for the most part. Scenarios F3, and F10, on the other hand, will remain more challenging to explore.

## 5 Conclusions

In light of null results from New Physics searches at the LHC, we look at unification of the gauge couplings as a model-building principle and classify possible SM extensions that feature this property.

As a first step, we considered in this study extensions of the SM with two distinct representations of VL fermions. We analyzed all their possible combinations with the number of fermions in each representation limited only by perturbativity of the gauge couplings at the unification scale. We found 13 different combinations of two representations that allow for precise gauge unification at energies higher than  $10^{15}$  GeV, and for VL masses in the range 0.25 – 10 TeV.

Interdependence between types of spectra required by the unification condition and their susceptibility to experimental tests is the main characteristics of successful PGU scenarios. We showed that the effectiveness of a given search in probing the allowed parameter space of a model is directly related to its two features: mass hierarchy among VL fermions and the value of the unification scale. Scenarios in which the colored fermions are much lighter than the non-colored ones may be almost entirely tested by the measurement of the running strong coupling and by the LHC  $R$ -hadron searches. And *vice versa*, if non-colored fermions are much lighter, HSCP searches and EW precision tests become very effective. On the other hand, scenarios in which both VL masses are of the same order remain beyond the reach of present-days colliders. In this case, however, null outcome from the proton decay experiments allows to exclude those models that feature the low unification scale.

The results presented in this study clearly highlight the importance of combining different experimental strategies in order to derive the most robust constraints on the PGU parameter space. In this regard, proton decay measurements play a particular role, as they offer the only mean of probing the VL spectra above the multi- TeV regime. There is also a great potential in the direct HSCP searches at the LHC. We hope that our results will prove useful for experimental collaborations in choosing benchmark BSM scenarios for their future analyses.

The current study can be extended in different directions. First of all, one may consider more complex (and more realistic) BSM scenarios, featuring for example more than two VL

representations or extra scalars. Secondly, the effects of non-gauge interactions (Yukawa and scalar types) should be taken into account, as they are bound to affect the phenomenology of PGU scenarios. After all, the desert seems like an interesting place to explore.

## ACKNOWLEDGMENTS

We would like to thank Enrico Sessolo for his comments on the manuscript. The use of the CIS computer cluster at the National Centre for Nuclear Research in Warsaw is gratefully acknowledged. This work is supported by the National Science Centre (Poland) under the research Grant No. 2017/26/E/ST2/00470.

## A Group invariants and beta functions

General two-loop beta functions for a system of gauge couplings  $g_i$  of a direct-product symmetry group  $G_i \times \dots$  read [38]

$$\begin{aligned} \beta_i = \frac{dg}{d \ln \mu} = & \frac{g_i^3}{(4\pi)^2} \left[ -\frac{11}{3}C_2(G_i) + \frac{2}{3}S_2(R_{Fi}) + \frac{1}{3}S_2(R_{Si}) \right] \\ & + \frac{g_i^5}{(4\pi)^4} \left[ -\frac{34}{3}C_2(G_i)^2 + \left(2C_2(R_{Fi}) + \frac{10}{3}C_2(G_i)\right)S_2(R_{Fi}) + \left(4C_2(R_{Si}) + \frac{2}{3}C_2(G_i)\right)S_2(R_{Si}) \right. \\ & \left. + \sum_{j=1}^k g_j^2 \left(2C_2(R_{Fj})S_2(R_{Fi}) + 4C_2(R_{Sj})S_2(R_{Si})\right) \right], \end{aligned} \quad (10)$$

where  $G_i$ ,  $R_{Fi}$  and  $R_{Si}$  denote contributions from gauge bosons, Weyl fermions, and complex scalars respectively.  $C_2(R)$  is a quadratic Casimir invariant,  $S_2(R)$  a Dynkin index of a representation  $R$ , and the sum is meant in both  $S_2(R_{Fi})$  and  $S_2(R_{Si})$  over all fermion and scalar representations transforming nontrivially under  $G_i$ .

The quadratic Casimir operator for the representation  $R$  of a symmetry group  $G$  is defined as

$$C_2(R)\delta_j^i = (t^A t^A)_j^i = \sum_{A=1}^d t^A t^A, \quad (11)$$

where  $t^A$  are the generators of  $G$  in the representation  $R$ . The Dynkin index of a representation  $R$  is instead given by

$$S_2(R)\delta^{AB} = \text{Tr} \{t^A t^B\}. \quad (12)$$

The two are related through the dimensions of the representation  $R$ ,  $d(R)$ , and of the adjoint,  $d(\text{Adj})$ ,

$$S_2(R)d(\text{Adj}) = C_2(R)d(R). \quad (13)$$

It is convenient to parameterize the quadratic Casimir operator, the Dynkin index, and the dimension of the representation through the weights  $(p, q)$  for irreducible  $SU(3)$  representations  $R_3$ , and, similarly, through the highest weight  $\ell$  for  $SU(2)$  representations  $R_2$ ,

$$\begin{aligned}
d(R_3) &= \frac{1}{2}(p+1)(q+1)(p+q+2), \\
C_2(R_3) &= p+q+\frac{1}{3}(p^2+q^2+pq), \quad \text{with } p, q = 0, 1 \dots, \\
d(R_2) &= 2\ell+1, \\
C_2(R_2) &= \ell(\ell+1), \quad \text{with } \ell = 0, \frac{1}{2}, 1 \dots.
\end{aligned} \tag{14}$$

The two-loop beta functions for the SM augmented with  $N_F$  fermions in the representation  $(R_{F3}, R_{F2}, Y_F)$  are straightforwardly derived from 10, and read

$$\beta_3 = \frac{g_3^3}{(4\pi)^2} B_3 + \frac{g_3^3}{(4\pi)^4} (C_{33} g_3^2 + C_{32} g_2^2 + C_{31} g_1^2), \tag{15}$$

$$\beta_2 = \frac{g_2^3}{(4\pi)^2} B_2 + \frac{g_2^3}{(4\pi)^4} (C_{23} g_3^2 + C_{22} g_2^2 + C_{21} g_1^2), \tag{16}$$

$$\beta_1 = \frac{g_1^3}{(4\pi)^2} B_1 + \frac{g_1^3}{(4\pi)^4} (C_{13} g_3^2 + C_{12} g_2^2 + C_{11} g_1^2), \tag{17}$$

with the one-loop coefficients determined as

$$B_3 = -7 + \frac{2}{3} N_F S_2(R_{F3}) d(R_{F2}), \tag{18}$$

$$B_2 = -\frac{19}{6} + \frac{2}{3} N_F S_2(R_{F2}) d(R_{F3}), \tag{19}$$

$$B_1 = \frac{41}{10} + \frac{2}{5} N_F d(R_{F3}) d(R_{F2}) Y_F^2. \tag{20}$$

The two-loop coefficients are given by

$$C_{33} = -26 + N_F S_2(R_{F3}) d(R_{F2}) (2C_2(R_{F3}) + 10), \tag{21}$$

$$C_{32} = \frac{9}{2} + 2N_F S_2(R_{F3}) C_2(R_{F2}) d(R_{F2}), \tag{22}$$

$$C_{31} = \frac{11}{10} + \frac{6}{5} N_F S_2(R_{F3}) d(R_{F2}) Y_F^2, \tag{23}$$

$$C_{23} = 12 + 2N_F S_2(R_{F2}) C_2(R_{F3}) d(R_{F3}), \tag{24}$$

$$C_{22} = \frac{35}{6} + N_F S_2(R_{F2}) d(R_{F3}) (2C_2(R_{F2}) + \frac{20}{3}), \tag{25}$$

$$C_{21} = \frac{9}{10} + \frac{6}{5} N_F S_2(R_{F2}) d(R_{F3}) Y_F^2, \tag{26}$$

$$C_{13} = \frac{44}{4} + \frac{6}{5} N_F C_2(R_{F3}) d(R_{F3}) d(R_{F2}) Y_F^2, \tag{27}$$

$$C_{12} = \frac{27}{10} + \frac{6}{5} N_F C_2(R_{F2}) d(R_{F2}) d(R_{F3}) Y_F^2, \tag{28}$$

$$C_{11} = \frac{199}{50} + \frac{18}{25} N_F d(R_{F3}) d(R_{F2}) Y_F^4. \quad (29)$$

## B Decomposition of the irreducible $SU(5)$ representations

In this Appendix we collected the branching rules for the embedding  $SU(5) \supset SU(3) \times SU(2) \times U(1)$  [55],

$$\begin{aligned}
\mathbf{5} &= (\mathbf{1}, \mathbf{2}, \frac{1}{2}) \oplus (\mathbf{3}, \mathbf{1}, -\frac{1}{3}), \\
\mathbf{10} &= (\mathbf{1}, \mathbf{1}, 1) \oplus (\bar{\mathbf{3}}, \mathbf{1}, -\frac{2}{3}) \oplus (\mathbf{3}, \mathbf{2}, \frac{1}{6}), \\
\mathbf{15} &= (\mathbf{1}, \mathbf{3}, 1) \oplus (\mathbf{3}, \mathbf{2}, \frac{1}{6}) \oplus (\mathbf{6}, \mathbf{1}, -\frac{2}{3}), \\
\mathbf{24} &= (\mathbf{1}, \mathbf{1}, 0) \oplus (\mathbf{1}, \mathbf{3}, 0) \oplus (\mathbf{8}, \mathbf{1}, 0) \oplus (\mathbf{3}, \mathbf{2}, -\frac{5}{6}) \oplus (\bar{\mathbf{3}}, \mathbf{2}, \frac{5}{6}), \\
\mathbf{35} &= (\mathbf{1}, \mathbf{4}, -\frac{3}{2}) \oplus (\bar{\mathbf{3}}, \mathbf{3}, -\frac{2}{3}) \oplus (\bar{\mathbf{6}}, \mathbf{2}, \frac{1}{6}) \oplus (\bar{\mathbf{10}}, \mathbf{1}, 1), \\
\mathbf{40} &= (\mathbf{1}, \mathbf{2}, -\frac{3}{2}) \oplus (\mathbf{3}, \mathbf{2}, \frac{1}{6}) \oplus (\bar{\mathbf{3}}, \mathbf{1}, -\frac{2}{3}) \oplus (\bar{\mathbf{3}}, \mathbf{3}, -\frac{2}{3}) \oplus (\mathbf{8}, \mathbf{1}, 1) \oplus (\bar{\mathbf{6}}, \mathbf{2}, \frac{1}{6}), \\
\mathbf{45} &= (\mathbf{1}, \mathbf{2}, \frac{1}{2}) \oplus (\mathbf{3}, \mathbf{1}, -\frac{1}{3}) \oplus (\mathbf{3}, \mathbf{3}, -\frac{1}{3}) \oplus (\bar{\mathbf{3}}, \mathbf{1}, \frac{4}{3}) \oplus (\bar{\mathbf{3}}, \mathbf{2}, -\frac{7}{6}) \oplus (\bar{\mathbf{6}}, \mathbf{1}, -\frac{1}{3}) \oplus (\mathbf{8}, \mathbf{2}, \frac{1}{2}), \\
\mathbf{50} &= (\mathbf{1}, \mathbf{1}, -2) \oplus (\mathbf{3}, \mathbf{1}, -\frac{1}{3}) \oplus (\bar{\mathbf{3}}, \mathbf{2}, -\frac{7}{6}) \oplus (\bar{\mathbf{6}}, \mathbf{3}, -\frac{1}{3}) \oplus (\mathbf{6}, \mathbf{1}, \frac{4}{3}) \oplus (\mathbf{8}, \mathbf{2}, \frac{1}{2}), \\
\mathbf{70} &= (\mathbf{1}, \mathbf{2}, \frac{1}{2}) \oplus (\mathbf{1}, \mathbf{4}, \frac{1}{2}) \oplus (\mathbf{3}, \mathbf{1}, -\frac{1}{3}) \oplus (\mathbf{3}, \mathbf{3}, -\frac{1}{3}) \oplus (\bar{\mathbf{3}}, \mathbf{3}, \frac{4}{3}) \oplus (\mathbf{6}, \mathbf{2}, -\frac{7}{6}) \oplus (\mathbf{8}, \mathbf{2}, \frac{1}{2}) \oplus (\mathbf{15}, \mathbf{1}, -\frac{1}{3}), \\
\mathbf{70}' &= (\mathbf{1}, \mathbf{5}, -2) \oplus (\bar{\mathbf{3}}, \mathbf{4}, -\frac{7}{6}) \oplus (\bar{\mathbf{6}}, \mathbf{3}, -\frac{1}{3}) \oplus (\bar{\mathbf{10}}, \mathbf{2}, \frac{1}{2}) \oplus (\bar{\mathbf{15}}', \mathbf{1}, \frac{4}{3}), \\
\mathbf{75}' &= (\mathbf{1}, \mathbf{1}, 0) \oplus (\mathbf{3}, \mathbf{1}, \frac{5}{3}) \oplus (\mathbf{3}, \mathbf{2}, -\frac{5}{6}) \oplus (\bar{\mathbf{3}}, \mathbf{1}, -\frac{5}{3}) \oplus (\bar{\mathbf{3}}, \mathbf{2}, \frac{5}{6}) \oplus (\bar{\mathbf{6}}, \mathbf{2}, -\frac{5}{6}) \oplus (\mathbf{6}, \mathbf{2}, \frac{5}{6}) \oplus \\
&\quad (\mathbf{8}, \mathbf{1}, 0) \oplus (\mathbf{8}, \mathbf{3}, 0).
\end{aligned} \quad (30)$$

## References

- [1] H. Georgi and S. L. Glashow, “Unity of All Elementary Particle Forces,” *Phys. Rev. Lett.* **32** (1974) 438–441.
- [2] J. C. Pati and A. Salam, “Lepton Number as the Fourth Color,” *Phys. Rev.* **D10** (1974) 275–289. [Erratum: *Phys. Rev.* **D11**, 703(1975)].
- [3] R. N. Mohapatra and J. C. Pati, “Left-Right Gauge Symmetry and an Isoconjugate Model of CP Violation,” *Phys. Rev.* **D11** (1975) 566–571.
- [4] H. Fritzsch and P. Minkowski, “Unified Interactions of Leptons and Hadrons,” *Annals Phys.* **93** (1975) 193–266.
- [5] H. Georgi, “The State of the Art Gauge Theories,” *AIP Conf. Proc.* **23** (1975) 575–582.
- [6] G. P. Cook, K. T. Mahanthappa, and M. A. Sher, “Effects of Heavy Colored Higgs Scalars on  $SU(5)$  Predictions,” *Phys. Lett.* **90B** (1980) 398–400.

- [7] V. V. Dixit and M. Sher, “The Futility of High Precision SO(10) Calculations,” *Phys. Rev.* **D40** (1989) 3765.
- [8] P. Langacker and N. Polonsky, “Uncertainties in coupling constant unification,” *Phys. Rev.* **D47** (1993) 4028–4045, [arXiv:hep-ph/9210235](#) [hep-ph].
- [9] K. Hagiwara and Y. Yamada, “Grand unification threshold effects in supersymmetric SU(5) models,” *Phys. Rev. Lett.* **70** (1993) 709–712.
- [10] J. Schwichtenberg, “Gauge Coupling Unification without Supersymmetry,” *Eur. Phys. J.* **C79** no. 4, (2019) 351, [arXiv:1808.10329](#) [hep-ph].
- [11] Y. Achiman and B. Stech, *New Phenomena in Lepton-Hadron Physics*. edited by D.E.C. Fries and J. Wess, Plenum, New York, 1979, p. 303.
- [12] A. de Rújula, H. Georgi, and S. L. Glashow, *Fifth Workshop on Grand Unification*. edited by K. Kang, H. Fried, and P. Frampton, World Scientific, Singapore, 1984, p. 88.
- [13] P. Fileviez Perez and S. Ohmer, “Low Scale Unification of Gauge Interactions,” *Phys. Rev.* **D90** no. 3, (2014) 037701, [arXiv:1405.1199](#) [hep-ph].
- [14] T. G. Rizzo, “Desert guts and new light degrees of freedom,” *Phys. Rev.* **D45** (1992) 3903–3905.
- [15] B. Zhang and H.-Q. Zheng, “Top quark, heavy fermions and the composite Higgs boson,” *Commun. Theor. Phys.* **35** (2001) 162–166, [arXiv:hep-ph/0003065](#) [hep-ph].
- [16] D. Choudhury, T. M. P. Tait, and C. E. M. Wagner, “Beautiful mirrors and precision electroweak data,” *Phys. Rev.* **D65** (2002) 053002, [arXiv:hep-ph/0109097](#) [hep-ph].
- [17] L.-F. Li and F. Wu, “Coupling constant unification in extensions of standard model,” *Int. J. Mod. Phys.* **A19** (2004) 3217–3224, [arXiv:hep-ph/0304238](#) [hep-ph].
- [18] D. E. Morrissey and C. E. M. Wagner, “Beautiful mirrors, unification of couplings and collider phenomenology,” *Phys. Rev.* **D69** (2004) 053001, [arXiv:hep-ph/0308001](#) [hep-ph].
- [19] G. F. Giudice and A. Romanino, “Split supersymmetry,” *Nucl. Phys.* **B699** (2004) 65–89, [arXiv:hep-ph/0406088](#) [hep-ph]. [Erratum: *Nucl. Phys.*B706,487(2005)].
- [20] I. Dorsner and P. Fileviez Perez, “Unification without supersymmetry: Neutrino mass, proton decay and light leptoquarks,” *Nucl. Phys.* **B723** (2005) 53–76, [arXiv:hep-ph/0504276](#) [hep-ph].
- [21] D. Emmanuel-Costa and R. Gonzalez Felipe, “Minimal string-scale unification of gauge couplings,” *Phys. Lett.* **B623** (2005) 111–118, [arXiv:hep-ph/0505257](#) [hep-ph].
- [22] R. Shrock, “Variants of the Standard Model with Electroweak-Singlet Quarks,” *Phys. Rev.* **D78** (2008) 076009, [arXiv:0809.0087](#) [hep-ph].

- [23] I. Gogoladze, B. He, and Q. Shafi, “New Fermions at the LHC and Mass of the Higgs Boson,” *Phys. Lett.* **B690** (2010) 495–500, [arXiv:1004.4217 \[hep-ph\]](#).
- [24] R. Dermisek, “Insensitive Unification of Gauge Couplings,” *Phys. Lett.* **B713** (2012) 469–472, [arXiv:1204.6533 \[hep-ph\]](#).
- [25] R. Dermisek, “Unification of gauge couplings in the standard model with extra vectorlike families,” *Phys. Rev.* **D87** no. 5, (2013) 055008, [arXiv:1212.3035 \[hep-ph\]](#).
- [26] I. Dorsner, S. Fajfer, and I. Mustac, “Light vector-like fermions in a minimal SU(5) setup,” *Phys. Rev.* **D89** no. 11, (2014) 115004, [arXiv:1401.6870 \[hep-ph\]](#).
- [27] M.-L. Xiao and J.-H. Yu, “Stabilizing electroweak vacuum in a vectorlike fermion model,” *Phys. Rev.* **D90** no. 1, (2014) 014007, [arXiv:1404.0681 \[hep-ph\]](#). [Addendum: *Phys. Rev.* **D90**, no. 1, 019901(2014)].
- [28] B. Bhattacharjee, P. Byakti, A. Kushwaha, and S. K. Vempati, “Unification with Vectorlike fermions and signals at LHC,” *JHEP* **05** (2018) 090, [arXiv:1702.06417 \[hep-ph\]](#).
- [29] N. Arkani-Hamed and S. Dimopoulos, “Supersymmetric unification without low energy supersymmetry and signatures for fine-tuning at the LHC,” *JHEP* **06** (2005) 073, [arXiv:hep-th/0405159 \[hep-th\]](#).
- [30] V. Barger, J. Jiang, P. Langacker, and T. Li, “String scale gauge coupling unification with vector-like exotics and non-canonical U(1)(Y) normalization,” *Int. J. Mod. Phys.* **A22** (2007) 6203–6218, [arXiv:hep-ph/0612206 \[hep-ph\]](#).
- [31] V. Barger, N. G. Deshpande, J. Jiang, P. Langacker, and T. Li, “Implications of Canonical Gauge Coupling Unification in High-Scale Supersymmetry Breaking,” *Nucl. Phys.* **B793** (2008) 307–325, [arXiv:hep-ph/0701136 \[hep-ph\]](#).
- [32] L. Calibbi, L. Ferretti, A. Romanino, and R. Ziegler, “Gauge coupling unification, the GUT scale, and magic fields,” *Phys. Lett.* **B672** (2009) 152–157, [arXiv:0812.0342 \[hep-ph\]](#).
- [33] I. Donkin and A. Hebecker, “Precision Gauge Unification from Extra Yukawa Couplings,” *JHEP* **09** (2010) 044, [arXiv:1007.3990 \[hep-ph\]](#).
- [34] C. Liu and Z.-h. Zhao, “ $\theta_{13}$  and the Higgs mass from high scale supersymmetry,” *Commun. Theor. Phys.* **59** (2013) 467–471, [arXiv:1205.3849 \[hep-ph\]](#).
- [35] S. Zheng, “Effective Higgs Theories in Supersymmetric Grand Unification,” *Eur. Phys. J.* **C77** no. 9, (2017) 588, [arXiv:1706.01071 \[hep-ph\]](#).
- [36] S. Zheng, “Minimal Vectorlike Model in Supersymmetric Unification,” [arXiv:1904.10145 \[hep-ph\]](#).
- [37] D. Buttazzo, G. Degrassi, P. P. Giardino, G. F. Giudice, F. Sala, A. Salvio, and A. Strumia, “Investigating the near-criticality of the Higgs boson,” *JHEP* **12** (2013) 089, [arXiv:1307.3536 \[hep-ph\]](#).

- [38] M. E. Machacek and M. T. Vaughn, “Two Loop Renormalization Group Equations in a General Quantum Field Theory. 1. Wave Function Renormalization,” *Nucl. Phys.* **B222** (1983) 83–103.
- [39] A. Perez-Lorenzana and W. A. Ponce, “GUTs and string GUTs,” *Europhys. Lett.* **49** (2000) 296–301, [arXiv:hep-ph/9911540](#) [hep-ph].
- [40] A. D. Bond, G. Hiller, K. Kowalska, and D. F. Litim, “Directions for model building from asymptotic safety,” *JHEP* **08** (2017) 004, [arXiv:1702.01727](#) [hep-ph].
- [41] P. Nath and P. Fileviez Perez, “Proton stability in grand unified theories, in strings and in branes,” *Phys. Rept.* **441** (2007) 191–317, [arXiv:hep-ph/0601023](#) [hep-ph].
- [42] **Super-Kamiokande** Collaboration, K. Abe *et al.*, “Search for proton decay via  $p \rightarrow e^+\pi^0$  and  $p \rightarrow \mu^+\pi^0$  in 0.31 megatonyears exposure of the Super-Kamiokande water Cherenkov detector,” *Phys. Rev.* **D95** no. 1, (2017) 012004, [arXiv:1610.03597](#) [hep-ex].
- [43] **Hyper-Kamiokande** Collaboration, K. Abe *et al.*, “Hyper-Kamiokande Design Report,” [arXiv:1805.04163](#) [physics.ins-det].
- [44] **CMS** Collaboration, V. Khachatryan *et al.*, “Measurement and QCD analysis of double-differential inclusive jet cross sections in pp collisions at  $\sqrt{s} = 8$  TeV and cross section ratios to 2.76 and 7 TeV,” *JHEP* **03** (2017) 156, [arXiv:1609.05331](#) [hep-ex].
- [45] **ATLAS** Collaboration, M. Aaboud *et al.*, “Search for heavy charged long-lived particles in the ATLAS detector in  $36.1 \text{ fb}^{-1}$  of proton-proton collision data at  $\sqrt{s} = 13$  TeV,” *Phys. Rev.* **D99** no. 9, (2019) 092007, [arXiv:1902.01636](#) [hep-ex].
- [46] M. Farina, G. Panico, D. Pappadopulo, J. T. Ruderman, R. Torre, and A. Wulzer, “Energy helps accuracy: electroweak precision tests at hadron colliders,” *Phys. Lett.* **B772** (2017) 210–215, [arXiv:1609.08157](#) [hep-ph].
- [47] **CMS** Collaboration, V. Khachatryan *et al.*, “Search for long-lived charged particles in proton-proton collisions at  $\sqrt{s} = 13$  TeV,” *Phys. Rev.* **D94** no. 11, (2016) 112004, [arXiv:1609.08382](#) [hep-ex].
- [48] **Particle Data Group** Collaboration, M. Tanabashi *et al.*, “Review of Particle Physics,” *Phys. Rev.* **D98** no. 3, (2018) 030001.
- [49] R. Barbieri, A. Pomarol, R. Rattazzi, and A. Strumia, “Electroweak symmetry breaking after LEP-1 and LEP-2,” *Nucl. Phys.* **B703** (2004) 127–146, [arXiv:hep-ph/0405040](#) [hep-ph].
- [50] G. Cacciapaglia, C. Csaki, G. Marandella, and A. Strumia, “The Minimal Set of Electroweak Precision Parameters,” *Phys. Rev.* **D74** (2006) 033011, [arXiv:hep-ph/0604111](#) [hep-ph].



- [51] D. S. M. Alves, J. Galloway, J. T. Ruderman, and J. R. Walsh, “Running Electroweak Couplings as a Probe of New Physics,” *JHEP* **02** (2015) 007, [arXiv:1410.6810](#) [hep-ph].
- [52] A. Falkowski and K. Mimouni, “Model independent constraints on four-lepton operators,” *JHEP* **02** (2016) 086, [arXiv:1511.07434](#) [hep-ph].
- [53] **ATLAS** Collaboration, G. Aad *et al.*, “Measurement of the double-differential high-mass Drell-Yan cross section in pp collisions at  $\sqrt{s} = 8$  TeV with the ATLAS detector,” *JHEP* **08** (2016) 009, [arXiv:1606.01736](#) [hep-ex].
- [54] **CMS** Collaboration, V. Khachatryan *et al.*, “Measurements of differential and double-differential Drell-Yan cross sections in proton-proton collisions at 8 TeV,” *Eur. Phys. J.* **C75** no. 4, (2015) 147, [arXiv:1412.1115](#) [hep-ex].
- [55] R. Slansky, “Group theory for unified model building,” *Physics Reports* **79** no. 1, (1981) 1 – 128. <http://www.sciencedirect.com/science/article/pii/0370157381900922>